Bulletin of the Seismological Society of America, Vol. 93, No. 1, pp. 139–151, February 2003

In Situ Evaluation of Shear-Wave Velocities in Seafloor Sediments with a Broadband Ocean-Bottom Seismograph

by Carlos Huerta-Lopez,* Jay Pulliam, and Yosio Nakamura

Abstract We present an *in situ* evaluation of the response of seafloor sediments to passive dynamic loads. Horizontal-to-vertical (H/V) spectral ratios are used to characterize local sediment response, and 1D wave propagation modeling is used to estimate soil properties and theoretical amplification factors of shallow sediment layers. Horizontal amplitudes increased by an order of magnitude at 0.35 Hz and by at least 2 orders of magnitude at 1.9 Hz relative to the vertical amplitude. A 50-m-thick soil system parameterized as three solid layers resting over a half-space with a water layer at the top produces theoretical H/V spectral ratios that are largely consistent with the observed H/V spectral ratios. Our modeling results were consistent between earthquake and background noise records. Modeling H/V spectral ratios of noise data recorded by a three-component broadband ocean-bottom seismograph (BBOBS) offers a fast and inexpensive method for site investigation in deep water with the potential of *in situ* seafloor sediment characterization, as well as local site effect studies for foundations (30–100 m) and pipelines (2–5 m) in deep water. One need not supply an active source or wait for an appropriate earthquake, and the BBOBS is small, inexpensive, and autonomous once deployed.

Introduction

Local soil conditions can have significant effects on the ground motions created by dynamic excitation, such as those generated by earthquakes. A given site may respond differently to various dynamic inputs, depending on the type of incident waves, the coherency of the incident wave field, and the direction of the waves' approach. However, if the wave field is incoherent and composed of waves coming from various directions, the site response would not vary significantly. Detailed knowledge of site conditions in terms of geometry, topography, sediment thickness, density, sediment velocity (stiffness), and sediment damping are essential to fully describe the physical processes involved in the site effect. Obtaining quantitative estimates of these physical parameters is complex but critical when designing strategic marine structures, such as drilling or production platforms or pipelines.

Local site effects resulting from dynamic input have been documented and studied by Kanai *et al.* (1956), Gutenberg (1957), Roësset and Whitman (1969), Aki (1988, 1993), Seale and Archuleta (1989), and Anderson *et al.* (1996), among others. Our discussion focuses on the effects of shallow soil layers in marine sediments on seafloor ground motion. We assess the local site effect of a Gulf of Mexico (GOM) location by characterizing horizontal-to-vertical (H/V) spectral ratios of background noise and earthquake time series recorded by the University of Texas Institute for Geophysics (UTIG) prototype broadband ocean-bottom seismograph (BBOBS). One-dimensional wave propagation modeling is performed using the modified Thomson-Haskell propagation matrix method (Thomson 1950; Haskell 1953), known as the stiffness matrix method developed by Kausel and Roësset (1981), in order to estimate physical properties and theoretical amplification factors of shallow soil layers. To our knowledge, the application described here is the first to address the problems of local site effect analysis and sediment characterization in marine environments using H/V spectral amplitude ratios.

Approaches to Characterizing Local Site Effects

In engineering seismology, studies of local site effects and site characterization are carried out by means of direct, *in situ* measurements of dynamic motions, as well as by numerical approaches, in which material properties are estimated by numerical modeling based upon available geotechnical information. Bard (1995) presented a general review of methodologies currently used to analyze local site effects. The main challenge of *in situ* measurements for site characterization is to remove source and path effects from observations. One approach to removing these effects, intro-

*Present address: Departamento de Sismología, Centro de Investigación Científica y de Educación Superior de Ensenada (CICESE), Km 107 Carretera Tijuana-Ensenada, Ensenada, 22860, B.C. México.

duced by Borcherdt (1970) and known as the reference site technique, consists of comparing spectral ratios of seismograms recorded simultaneously at nearby sites. Source and path effects are assumed to be identical for the records at both sites. This technique is limited to sites for which additional stations are located nearby, such as stations of a dense local network.

A second popular approach, broadly known as non–reference site techniques, includes (1) parameterized source and path inversion (Field and Jacob, 1995) and (2) modeling spectral ratios between the horizontal and the vertical components of the wave field. Thomson (1950) and Haskell (1953) introduced an elegant formalism for studying wave propagation in layered media based on the use of transfer matrices in the frequency-wavenumber domain. Horvath *et al.* (1980) compared experimental H/V spectral ratios obtained from long-period moonquake seismograms with theoretical H/V spectral ratios calculated with the Haskell matrix to determine the shallow shear-wave velocity of the Moon. Nakamura (1989) introduced the H/V spectral ratio of noise records (microtremors) and proposed, based on empirical observations, that the H/V spectral ratio is a reliable estimation of the site response to *S* waves. He argued that dividing the horizontal spectra by the vertical spectral "reference" component removes source effects as well as the effects of Rayleigh waves, since these contributions are common to both components. The basic assumption is that local site conditions do not significantly influence the vertical component of ground motion. This technique has been applied to weak and strong ground motions by Acosta *et al.* (1994), Theodulidis and Bard (1995), Theodulidis *et al.* (1996), and Raptakis *et al.* (1998), among others. These researchers reported that results obtained with H/V spectral ratios are more stable than those obtained with raw noise spectra. In addition, H/V spectral ratios clearly define resonance peaks at soft soil sites, which indicate the sites' preferential vibration modes and reveal the overall frequency dependence of the site response. However, H/V spectral ratios often fail to identify higher harmonics, and the frequency peaks' amplitudes are different from the amplification measured on ratios of spectra for two different sites. Although Nakamura's technique lacks analytical and theoretical support (Lachet and Bard, 1994) and discriminates source and Rayleigh-wave effects from pure site effects only crudely, its simplicity, inexpensiveness, and the successful results reported in the literature support its use.

Given the cost of conducting active source experiments in the oceans, the dearth of nearby reference sites available for studies, and the great cost of drilling the seafloor, we chose to apply and evaluate Nakamura's technique to data recorded at a single site in the GOM. We also modeled the H/V spectral ratios using the modified Thomson-Haskell propagator matrix technique, known as the stiffness matrix method (Kausel and Roësset, 1981), and a 1D, layered soil system. Although more sophisticated numerical modeling approaches are now available that better represent complex "real world" sites as well as the true complexity of the incident wave field, simple 1D wave propagation techniques often provide satisfactory results for establishing design criteria and are used routinely in engineering practice. The objectives of analyzing local site effects were (1) to identify at which frequencies the spectral amplitudes were enhanced by the effect of the shallow 30- to 50-m soft sediments of the GOM seafloor, (2) to characterize the site in terms of its fundamental resonant frequency, and (3) to characterize the site in terms of its physical properties.

Instrumentation

A three-component broadband sensor PMD-2123 was installed in the ocean-bottom seismograph (OBS) package of the UTIG (BBOBS). Rather than the traditional force-balance pendulum design, the PMD sensor is based on a molecular-electronic transducer (MET) as the mechanism to detect ground motions (Abramovich *et al.*, 2001). This sensor provides (1) a wideband frequency response (0.033–30 Hz), (2) portability, (3) low power consumption (5 mA), (4) tolerance to tilt (up to 5°), and it is completely sealed (isolating it from variations in atmospheric pressure). The gain of the UTIG OBS recording package is dynamically adjusted ("gain-ranged") by software instructions to utilize the full range of the 14-bit analog-to-digital converter (ADC), yet clipping of large-amplitude signals is avoided. A complete description of the UTIG OBS characteristics can be found in Nakamura and Garmany (1991). The OBS with broadband sensor installed is useful not only for characterizing local site effects of marine layered systems, but also for regional and teleseismic broadband seismology (Pulliam *et al.*, 2003).

Gulf of Mexico Experiment

The GOM data were acquired in the summer of 1999 on the midslope of the northwestern GOM. This site was selected for deployment because (1) it is flat over a sufficiently broad area to accommodate the instrument; (2) the area has sedimentary evidence of recent structural activity, likely to have been caused by tectonically active salt domes (Satterfield and Behrens, 1990); (3) it is near a teleseismically determined earthquake epicenter (Frohlich, 1982); and (4) it is on the midcontinental slope, deep enough to avoid being caught in a fishing net. Figure 1 shows the location of the GOM experimental site and the locations of nearby, permanently moored weather buoy stations operated by the National Oceanic and Atmospheric Administration (NOAA).

Once the BBOBS was deployed and the instrument had settled on the seafloor at 1478 m below sea level, we shot two short crossing seismic lines over the instrument using a small (60 $inch^3$, 1.0 L) air gun for the purpose of locating and orienting the instrument using water wave arrivals (Nakamura *et al.*, 1987). The BBOBS was programmed to record three channels at 40 samples/sec for 4 weeks. On the day of

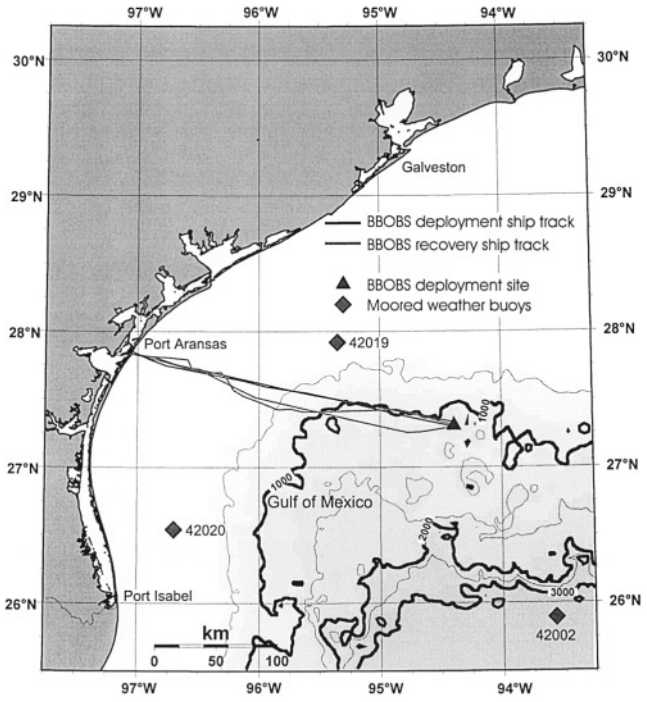

Figure 1. Experimental site and NOAA moored-buoy weather stations in the Gulf of Mexico. Cruises to deploy and recover the BBOBS occurred in July and August of 1999, respectively, aboard the R/V *Longhorn*. The BBOBS was deployed in a water depth of 1498 m in a flat basin on the midslope. Bathymetric depths are in meters. See text for further details.

recovery we repeated the crossing lines while shooting the small air gun, then sent an acoustic signal to release the instrument from its anchor on the seafloor. Upon recovery, the BBOBS was found to have operated normally, and data were obtained for the full 28-day deployment.

Data Processing

Simulated drum records of seafloor ground motion versus time were first plotted for visual inspection. The visual inspection was mainly concerned with the selection of the desired types of signals to be used in the frequency domain analysis, which consisted of power spectral density (PSD) estimates of the time series. For the background noise analysis we avoided time periods with transient signals, such as seismic events, bumps, and glitches. Roughly 30 regional and teleseismic events appeared clearly on these records (Pulliam *et al.*, 2003).

To convert from digital units (DU) to physical units of ground motion in velocity (m/s) we used the nominal conversion factor of 2.6×10^{-9} (m/s)/DU of the whole system, including sensor and recording package, since the instrument response is flat over the entire frequency range (0.033–10 Hz) considered in this study. PSD spectral estimates were obtained for each 36 m 16 s time series (87,040 samples) of background noise by dividing it into 82 subsegments of 4096 samples each, with an overlap of 75%. The mean value was removed, and a Hanning window of 4096 points was applied to each subsegment. The averaged PSD estimates were then normalized, and after the instrument correction was applied the spectral amplitudes were transformed to units of acceleration. For cases in which the entire day was analyzed, we divided the day into four intervals of approximately 6 hr each, starting at midnight. Each interval was formed by 10 segments of 36 m 16 s each. For the whole day, the total number of samples was 3,481,600 per channel.

Modeling H/V Spectral Ratio via the Stiffness Matrix Method

Consider a layered soil system, isolate a single layer and preserve equilibrium by applying external loads at the upper and the lower interfaces. Then, from $Z_{j+1} = H_j Z_j$ (Kausel and Roësset, 1981),

$$\begin{Bmatrix} \vec{D}_2 \\ \vec{\tau}_2 \end{Bmatrix} = \begin{bmatrix} H_{11} & H_{12} \\ H_{21} & H_{22} \end{bmatrix} \begin{Bmatrix} \vec{D}_1 \\ \vec{\tau}_1 \end{Bmatrix}, \tag{1}$$

where $\vec{\tau}_1$ and $\vec{\tau}_2$ are the external traction vectors at the upper and lower interfaces, respectively, H_{ij} are submatrices of the transfer matrix H_j, and $\vec{D}_1$ and $\vec{D}_2$ are the displacement vectors at the respective upper and lower interfaces. After some matrix algebra,

$$\begin{Bmatrix} \vec{\tau}_1 \\ \vec{\tau}_2 \end{Bmatrix} = \begin{bmatrix} -H_{12}^{-1}H_{11} & H_{12}^{-1} \\ H_{22}H_{12}^{-1}\ H_{11} - H_{21} & -H_{22}H_{12}^{-1} \end{bmatrix} \begin{Bmatrix} \vec{D}_1 \\ \vec{D}_2 \end{Bmatrix}, \tag{2}$$

or in compact notation $\vec{L} = K\vec{D}$, where K is the stiffness matrix of the layer, $\vec{L}$ is the external load vector, and $\vec{D}$ is the displacement vector. For a layered soil system, the global stiffness matrix is constructed by overlapping the contribution of the layer matrices at each interface of the system. The global load vector then corresponds to the prescribed external tractions at the outermost interfaces. In the following, the stiffness matrix approach for a single layer is described for an *SH* wave propagating from bottom to top. This is also known as the antiplane, or out-of-plane, problem. The reader should consult Kausel and Roësset (1981) for a complete derivation of the stiffness matrix for the whole wave field, for a single layer, or for multilayered soil systems.

The antiplane problem considers a traveling wave restricted to the *x*-*z* plane, as is schematically illustrated in Figure 2. In this figure, α_i denotes the angle of incidence of the incoming wave, and α_r the refracted angle of the wave inside the layer; l and n are the direction cosines for the displacements V inside the layer, A_{SH} and A'_{SH} represent the amplitudes of *SH* waves traveling in the positive and negative directions of the z axis; and C_s, ρ, ξ, and σ are the shear-wave velocity, density, material damping ratio, and the Poisson's ratio of the soil layer, respectively. The following equation represents the relationship between the stresses and

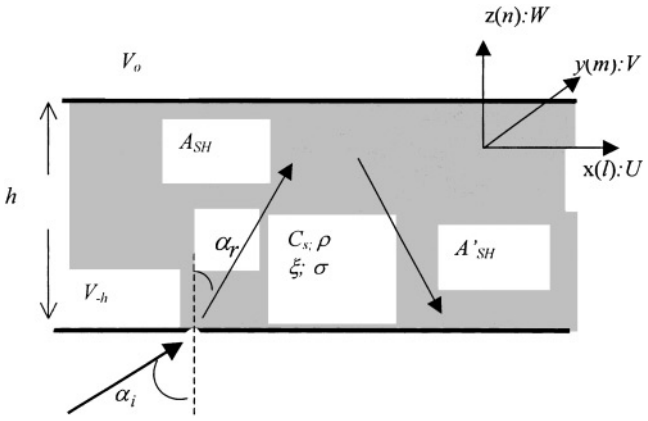

Figure 2. *SH* wave traveling in a single layer resting over a half-space.

displacements from the bottom to the top of a single layer through the propagator stiffness matrix:

$$\begin{Bmatrix} \tau_o \\ \tau_{-\mathrm{h}} \end{Bmatrix} = \frac{Gks}{e^{ksh} - e^{-ksh}} \begin{bmatrix} e^{ksh} + e^{-ksh} & -2 \\ -2 & e^{ksh} + e^{-ksh} \end{bmatrix} \begin{Bmatrix} V_o \\ V_{-h} \end{Bmatrix} \tag{3}$$

where G is the elastic shear modulus, k the horizontal wavenumber, s a complex number as defined below, and the product of the first two factors of the right-hand side of the above equation is the dynamic stiffness matrix (K) of a single layer for antiplane *SH* wave. Using some trigonometric identities the stiffness matrix can be written in compact form:

$$K_{k\neq 0} = \frac{Gks}{\sinh(ksh)} \begin{bmatrix} \cosh(ksh) & -1 \\ -1 & \cosh(ksh) \end{bmatrix}, \tag{4}$$

where

$$s = i\frac{n}{1} = i\frac{\cos(\alpha_r)}{\sin(\alpha_r)} = \sqrt{1 - \frac{\omega^2}{(kC_s)^2}}, \quad \text{and}$$

$$k = \frac{\omega l}{C_s} = \frac{\omega \sin(\alpha_r)}{C_s}.$$

The stiffness matrix method was applied to the GOM data because (1) it has the freedom to use the whole field of waves (*P, SV*, and *SH*) or the independent seismic waves that may be of interest, (2) it is well suited to model thin layers, (3) it can handle any incident angle of the input wave motion at the base of the layered system, and (4) one can easily follow the evolution of the wave field as it passes through the interfaces of the layered soil system.

Experimental and Numerical Results

Correlation to Weather Conditions

In an effort to determine the sources of the ambient noise recorded on the seafloor, we first examined the correlation between the power of the background noise and the weather observables (measurements of wave height, wind gusts, wind direction, dominant wave period, and average wave period) recorded at the sea surface. We used data from three permanently moored weather buoys (Fig. 1) located in the vicinity of the BBOBS GOM site. Buoys 42019 (116 km northwest of GOM site, water depth of 86 m) and 42002 (at 176 km southeast of GOM site, water depth of 3200 m) were closest to the GOM site. Weather data were obtained from the NOAA's web site (*www.ndbc.noaa.gov/stuff/westgulf*). Figure 3 shows the power estimate at buoy 42019 for the related time series compared with the power estimate of the background noise of the vertical component recorded by the BBOBS. BBOBS power was computed as the mean squared amplitude value of 68 sec windows with no overlap. In an effort to determine sources of BBOBS noise, seismic events and transients were excluded from the time series for the purposes of power estimation.

From the comparison of data sets, it is clear that wave height and wind speed correlate best with the seismic background noise recorded by the BBOBS. Figure 4 shows these correlations in detail for stations 42019 and 42002 versus all three components of BBOBS data. Figure 4 also shows a time lag in the correlations between wind speed and BBOBS power, indicating a delay in response of seafloor sediments to variations in wind conditions at the sea surface, but virtually no time lag of BBOBS power with respect to wave height. It appears that, while it takes some time for waves to build or dissipate in response to changes in wind speed, once average and peak wave heights have increased (or decreased), the changes in noise conditions are transmitted immediately to the BBOBS on the seafloor.

Experimental H/V Spectral Ratios

Both background noise and earthquakes were used as sources of weak and moderate ground motions and also of presumably nondirectional and directional signals, respectively. We first computed spectral ratios of background noise time series with different power levels, which are indicated in Figure 4 on days 201 and 205 for high and low power levels, respectively. The different power levels were also evident in the PSD spectral amplitude levels. The H/V spectral ratios of the time series with high and low power are shown in Figure 5a and b, respectively. The H/V spectral ratios obtained with the low power level time series do not define the 1.9-Hz peak as well as the higher power ratios. Averaging a large number of background noise series increases the signal-to-noise ratio, produces smoother curves, and improves the definition of the resonance peaks at 1.9, 3.9, and 6.3 Hz, which can be associated with local site effect (Figs. 5c, d).

In order to compare H/V spectral ratios obtained with background noise to those obtained with stronger energy sources, we computed H/V spectral ratios for transient arrivals due to earthquakes as well. Of the four earthquakes used in this analysis (Table 1), two had the same magnitude (m_b

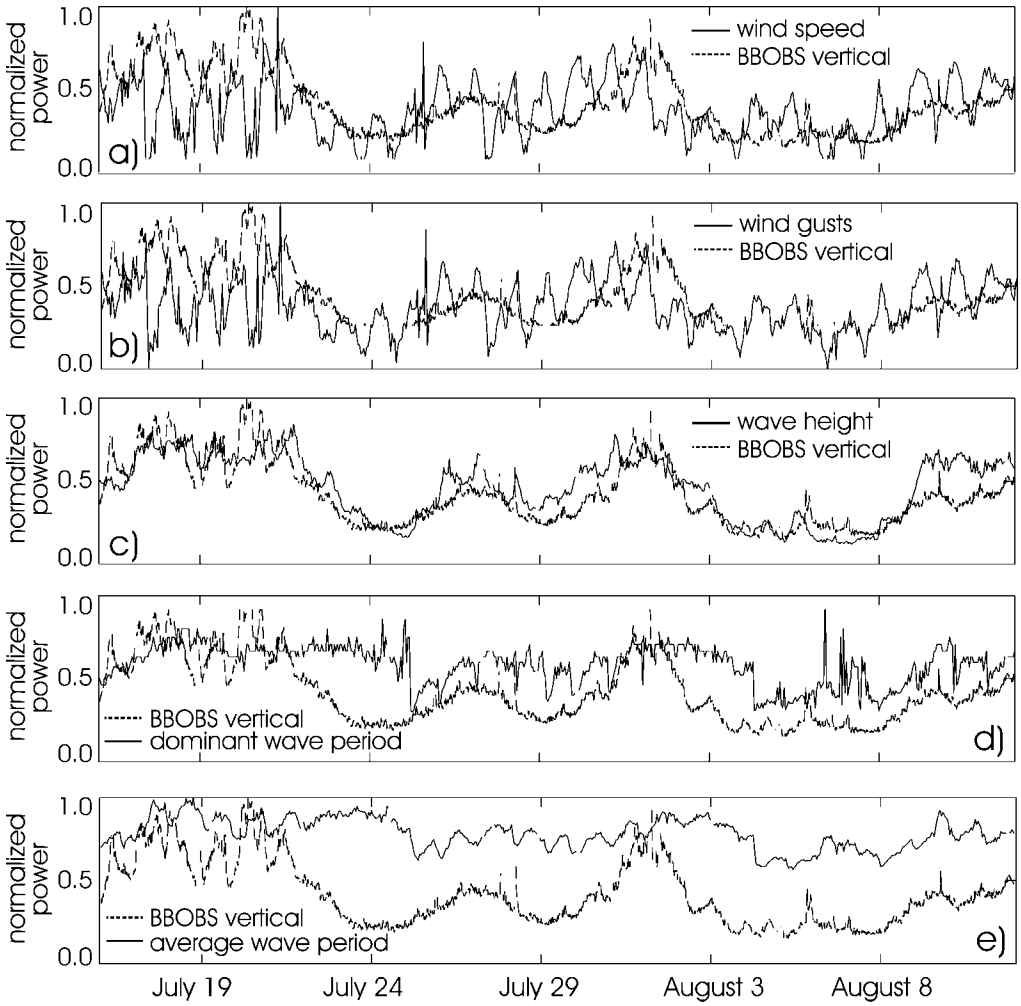

Figure 3. Comparison of normalized "power" (squared amplitude) of various weather observables recorded at NOAA buoy weather station 42019 with "power" of BBOBS background noise recorded on the seafloor at the GOM site (Fig. 1). Transient signals have been removed from the BBOBS time series.

= 5.1). One of these two was located in the Gulf of California, the other in the California-Nevada border region, at epicentral distances of 13.3° and 21.5° from the GOM site, respectively. The third and fourth earthquakes were located in Ecuador (m_b = 5.9, Δ = 33.89°) and Nicaragua (m_b = 4.9, Δ = 16.45°), respectively (Fig. 6). General characteristics of the H/V spectral ratios obtained with earthquake signals are shown in Figure 7a–d. Note, however, that the H/V spectral ratios obtained for the California-Nevada region and Nicaragua earthquakes do not show the 3.9 and 6.5 Hz peaks. These peaks are well defined in the ratios obtained with background noise and with the Gulf of California and Ecuador earthquakes. This discrepancy could be produced by differences in energy levels at frequencies greater than 2.3 Hz, which could be caused by source directivity or by differences in earthquake magnitudes or epicentral distances. Another potential explanation is a 3D effect, such as lateral heterogeneity or anisotropy, that causes the incident wave field to violate the fundamental assumption of Nakamura's technique, that vertical motion is decoupled from horizontal motion. These issues are addressed further in the Discussion section below.

Modeling the Local Site Response of GOM Site

To characterize the local site response of the experimental GOM site, the upper 50-m-deep sedimentary layer of the GOM seafloor was modeled as a system composed of three constant velocity layers resting over a half-space. In this model, the water "layer" of 1475 m was added to the top of the seafloor to better simulate GOM site conditions. The model thus was a four-layer system in which the uppermost layer was water. Initial and final model parameters are given in Table 2.

The forward modeling process was started by propagating vertically incident *P, SV*, and *SH* waves through the vertical column. Theoretical H/V spectral ratios at the desired

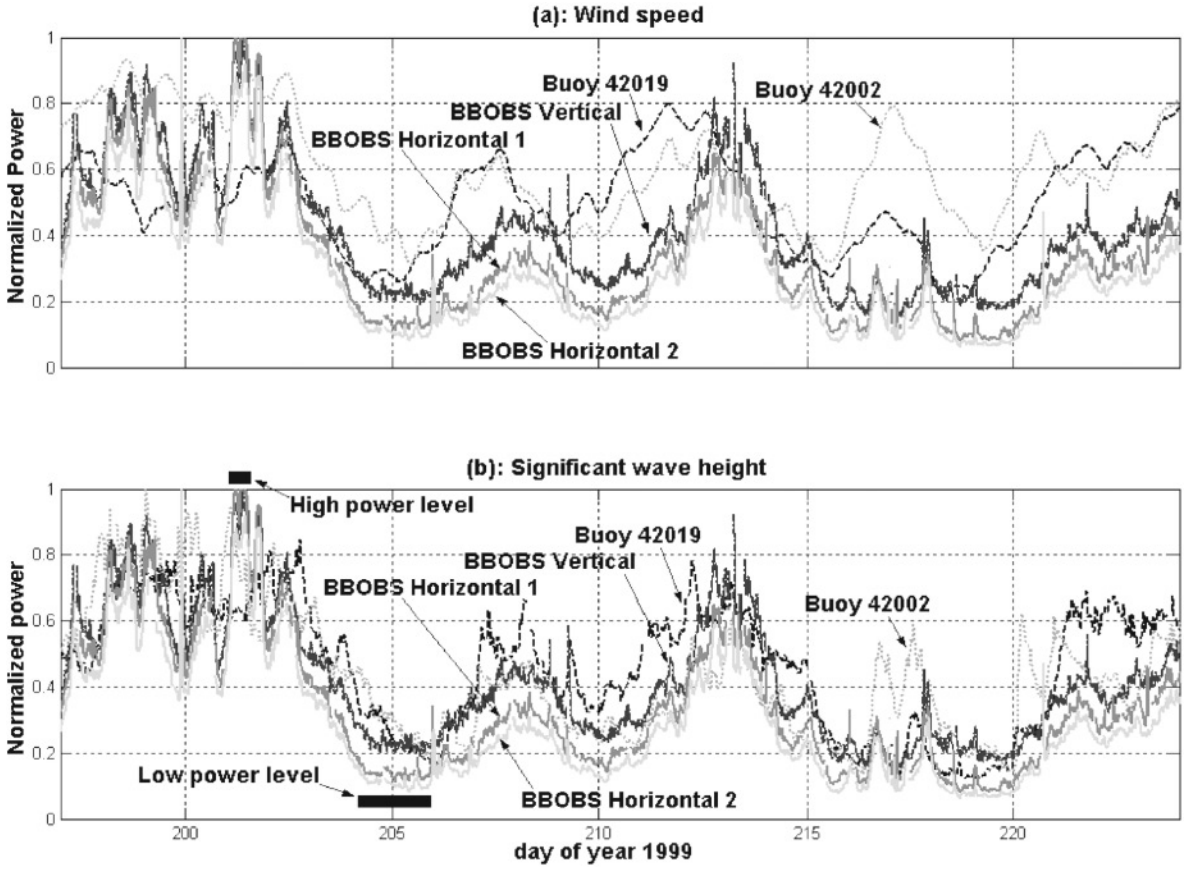

Figure 4. (a) The "power" (squared amplitude) of BBOBS background noise with transient signals removed correlates well with wind speed, as recorded at the sea surface by buoys 42019 and 42002 (Fig. 1), but there is a time lag associated with the correlation. (b) The strongest correlation is between BBOBS power and "significant wave height" (the highest wave recorded in each 15-min period) at the sea surface. Horizontal 1 is oriented 42.8° east of north; horizontal 2 is oriented 132.8° east of north.

interfaces were calculated and compared with the observed ratios computed with time series of both background noise and earthquakes. The forward modeling process was iterated, varying the physical properties of the model, until the theoretical H/V spectral ratios that best fit the experimental H/V spectral ratios (under the least-squares criterion) were found. At early iterations, the layer's thickness, Poisson's ratio, density, shear modulus, and damping coefficient were each varied. At later iterations, after coarse characteristics of the observed spectral ratios were matched reasonably well, layer thickness and Poisson's ratio were held fixed and only density, shear modulus, and damping coefficient were perturbed. For fine-tuning the matching between the theoretical and the experimental H/V spectral ratios, in a second step the incidence angle was varied until the best fit was found. A 30° incident *P* wave produced the best results in matching the theoretical and experimental H/V spectral ratios. The forward modeling process was quite successful. Figures 5 and 7 show that there is good agreement between the computed and observed H/V spectral ratios for both background noise and earthquakes, particularly at the 1.9 Hz peak.

To evaluate our results, we first examined Nakamura's hypothesis, that is, that the vertical component is not significantly influenced by the contribution of converted shear waves in the shallowest layers (softest sediments). For this to be true, the time series of background noise recorded on horizontal components should be relatively incoherent with respect to the time series recorded on the vertical component. Only then will the H/V spectral ratios isolate shear modes from coupled *P-SV* energy. The coherence of horizontal versus vertical was computed using the background noise time series with low, mid, and high power levels, described in the previous section. Figure 8 plots the coherence of horizontal versus vertical components for background noise with low power level. In all three cases, we find low coherence in the frequency band 0.03–3 Hz. It is within this band that the observed and theoretical H/V spectral ratios match best, with the exception of the ramp in the observed spectra from 0.05 to 1.5 Hz. A better match might be obtained in this latter frequency band if deeper structure were considered as well. This speculation will be tested with a more sophisticated, automated modeling approach, which will be the subject of

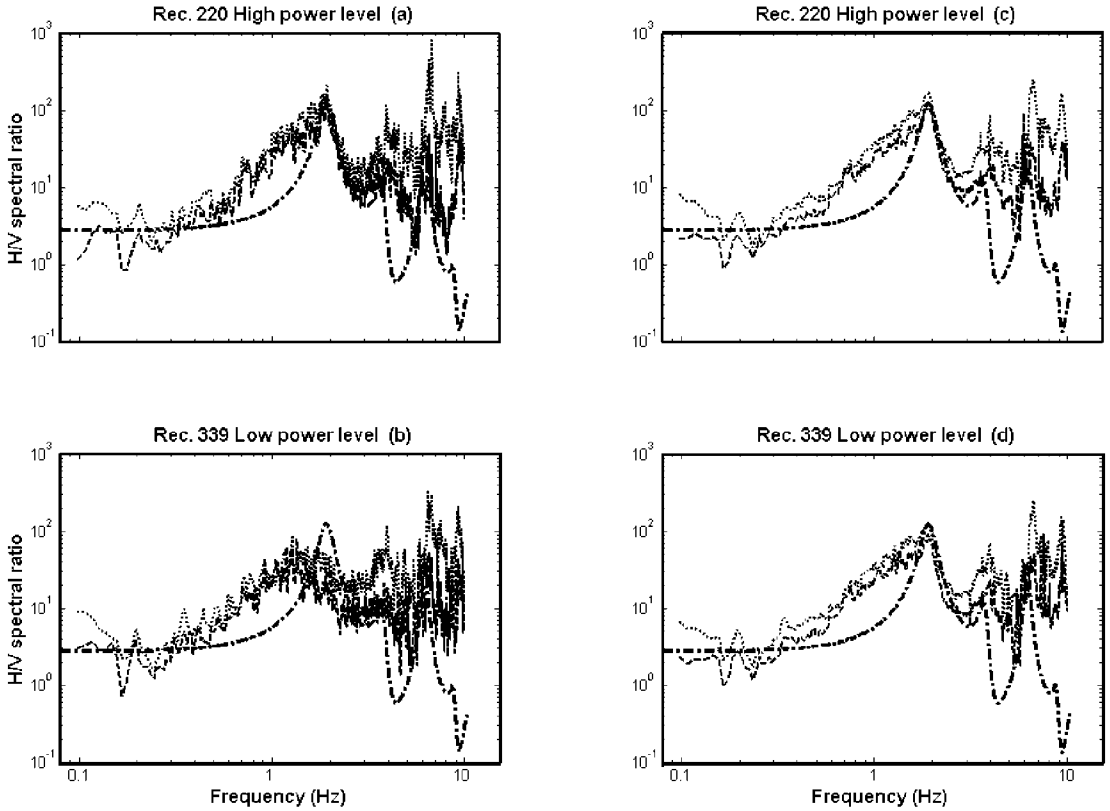

Figure 5. Theoretical and experimental H/V spectral ratios obtained with a single 36 m 16 s segment (87,040 samples, average of 82 subsegments of 4096 samples each) of background noise for (a) a relatively noisy period and (b) a relatively quiet period and ratios obtained with multiple 36 m 16 s segments for the same (c) noisy (29 segments of 87,040 samples, average of 2378 subsegments of 4096 samples each) and (d) quiet periods (48 segments of 87,040 samples, average of 3936 subsegments of 4096 samples each). Days with high and low power are indicated on Figure 4b. The dashed line is H1/V (H1 is oriented 42.8° east of north); the dotted line is H2/V (132.8° east of north). The dash-dot line is the theoretical H/V spectral ratio, which is computed with a 1D model and is therefore independent of orientation in the horizontal plane.

Table 1
Parameters of Earthquakes Used in This Study

Date (m/d/y)	Origin time (h:m:s)	Latitude	Longitude	Depth (km)	Mag.	Epicentral Distance	Region
7/16/99	13:45:25.5	23.775° N	108.708° W	10	5.1 m_b	13.3°	Gulf of California
8/02/99	06:05:13.0	37.380° N	117.070° W	3	5.1 m_b	21.5°	California–Nevada
8/03/99	15:58:57.6	3.453° S	79.162° W	88	5.9 M_l	33.9°	Coast of Ecuador
8/05/99	07:11:15.7	12.343° N	86.724° W	10	4.9 m_b	16.5°	Nicaragua

Mag., Magnitude; m_b, body-wave magnitude; M_l, local magnitude.

future work. At frequencies higher than 3.8 Hz the coherence increases sharply to a value of 0.6. We interpret the increased coherence at frequencies above 3.8 Hz as resulting from a significant contribution of converted shear modes. Perhaps *P-SV* conversion is more efficient in this band. The increase in coherence at higher frequencies is a typical pattern throughout the data set, but the frequency at which coherence begins to increase varies during the deployment. As noted above, high coherence violates a basic assumption of the H/V spectral ratio method and renders the modeling performed at coherent frequencies unreliable. However, tests in which model parameters are known independently must be performed before one can determine at what level of coherence the H/V spectral ratios fail to largely represent shear modes. A coherence of 0.6, though significantly different from the nearly zero coherence at lower frequencies, does not necessarily invalidate the modeling results.

Once the final model (Table 2) whose theoretical H/V

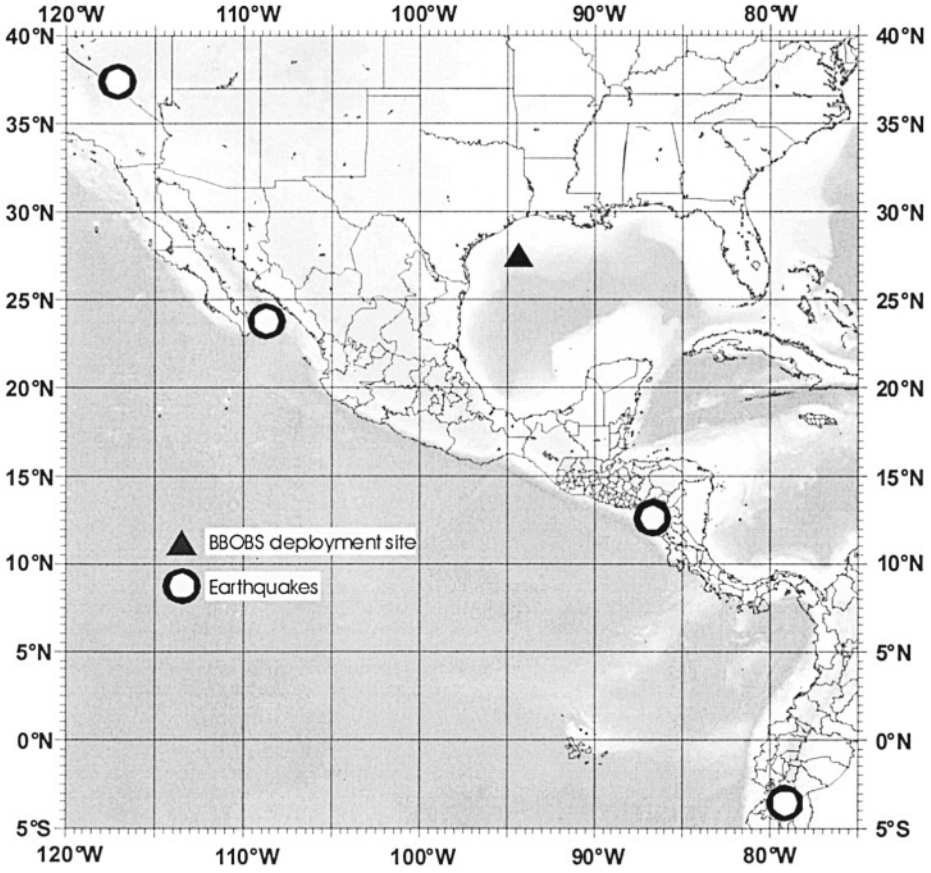

Figure 6. Location of earthquakes used in this study (see Table 1).

spectral ratios best matched the observed H/V spectral ratios was determined, transfer functions were computed for an *SH* wave traveling in (1) each individual layer of the discrete sediment model (Fig. 9a–c), (2) the cumulative contribution of the first and second layers (Fig. 9d, i.e., the top 15 m), as well as the second and third layers (Fig. 9e); and (3) the entire 50-m soil system that best represents the experimental GOM site (Fig. 9f). The following characteristics in Figure 9 are noted: (1) the top 5 m of the marine sediments has a single amplification peak at 4.5 Hz (Fig. 9a); (2) for the second 10-m-thick layer, the amplification peaks are at 2.9 and 6.2 Hz, while a deamplification trough is at 4.5 Hz (Fig. 9b); (3) three significant amplification peaks for the 35-m-thick third layer are located at 1.9, 3.8, and 9 Hz, and one significant deamplification trough is at 6.2 Hz (Fig. 9c); (4) the cumulative effect of the upper 15 m (the first and second layers) shows two single-amplification peaks at 2.9 and 6.2 Hz, which significantly reduce the amplification of the upper 5-m-thick layer (Fig. 9d); (5) the cumulative effect of the second and third layers (45 m in total thickness) shows amplification peaks at 1.9, 3.9, 6.2, and 9 Hz, and a single deamplification trough at 4.5 Hz (Fig. 9e); and (6) the transfer function of the upper 50 m, the whole three-layer sediment system, shows four amplification peaks at 1.9, 3.9, 6.2, and 9 Hz.

An examination of transfer functions of individual layers allows us to identify the contributions of each layer to enhancing or suppressing spectral amplitudes of the entire soil system. These transfer functions characterize preferential vibrational modes of the site, not only at the surface, but also at depth. They provide design criteria for engineering marine structures and therefore have direct practical applications. They also offer insight into the sensitivity of modeling results to perturbations to model parameters. The offset of a large amplification peak in a given layer by a large deamplification peak in another layer suggests that relatively small changes in physical properties or thickness, which perturb the layer's amplification peak only slightly, can result in a new and significantly different cumulative transfer function emerging from the stack of layers.

Discussion

In this study we measured seafloor ground motion at the experimental GOM site using a broadband seismograph and calculated H/V spectral ratios in the frequency band 0.1–10 Hz. The H/V spectral ratios were then used to evaluate local site effects caused by soft marine sediments via numerical modeling performed with the stiffness matrix method of Kausel and Roësset (1981). High-amplitude "peaks" in the

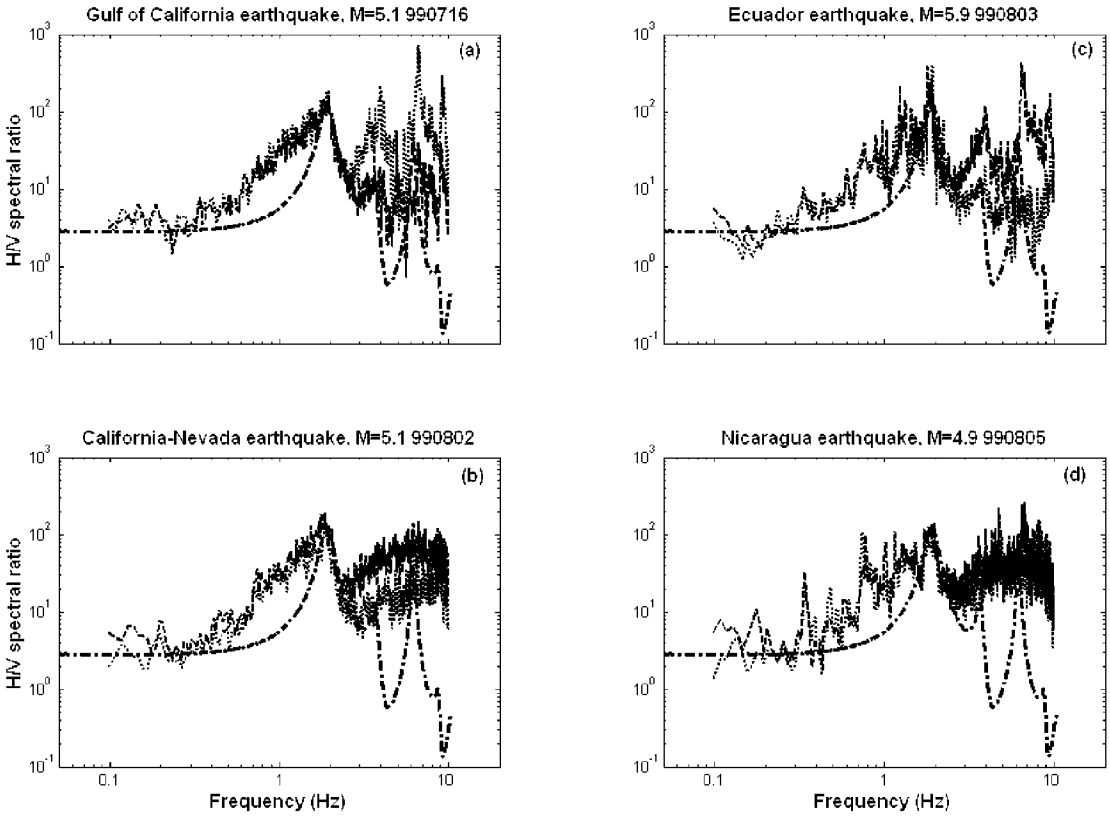

Figure 7. H/V spectral ratios for the (a) Gulf of California and (c) Ecuador earthquakes show clear peaks at 3.9 and 6.5 Hz, as well as the fundamental mode at 1.9 Hz. Spectral ratios for the (b) California-Nevada and (d) Nicaragua earthquakes do not show the higher frequency peaks. Table 1 lists the parameters of these earthquakes. The dashed line is H1/V (H1 is oriented 42.8° east of north); the dotted line is H2/V (132.8° east of north). The dash-dot line is the theoretical H/V spectral ratio.

Table 2
Initial and Final Model Parameters

Layer Thickness (m)	V_s (m/sec)	Density (ρ) (kg/m^3)	Shear Modulus (G) (N/m^2)	Damping (ξ) Fraction	Poisson's Ratio (σ)
Initial Parameters					
1475	~0	1000	0.0000E+00	0.1	0.50
5	180	1500	0.4860E+08	0.2	0.45
10	200	1600	0.6400E+08	0.1	0.40
35	400	1900	0.3040E+09	0.1	0.35
∞	1500	2500	0.5625E+10	0.000	0.25
Final Parameters					
1475	~0	1000	0.0000E+00	0.001	0.50
5	90	1300	0.1053E+08	0.01	0.45
10	190	1400	0.5054E+08	0.005	0.40
35	400	1700	0.2720E+09	0.005	0.35
∞	3000	2100	0.1890E+11	0.000	0.25

Layer thickness and Poisson's ratio are fixed parameters in the modeling process.

experimental H/V spectral ratios, obtained with either background noise or earthquakes, were interpreted as the preferential vibration modes of the layered sediment system. These results were consistent with the theoretical H/V spectral ratios computed for a model consisting of four layers over a half-space in which the topmost layer is water, particularly at the 1.9, 3.9, and 6.5 Hz resonance peaks. The mismatch between observed and theoretical H/V spectral ratios in frequency ranges that have high coherence may be explained by the fact that *SV*-type waves are significantly

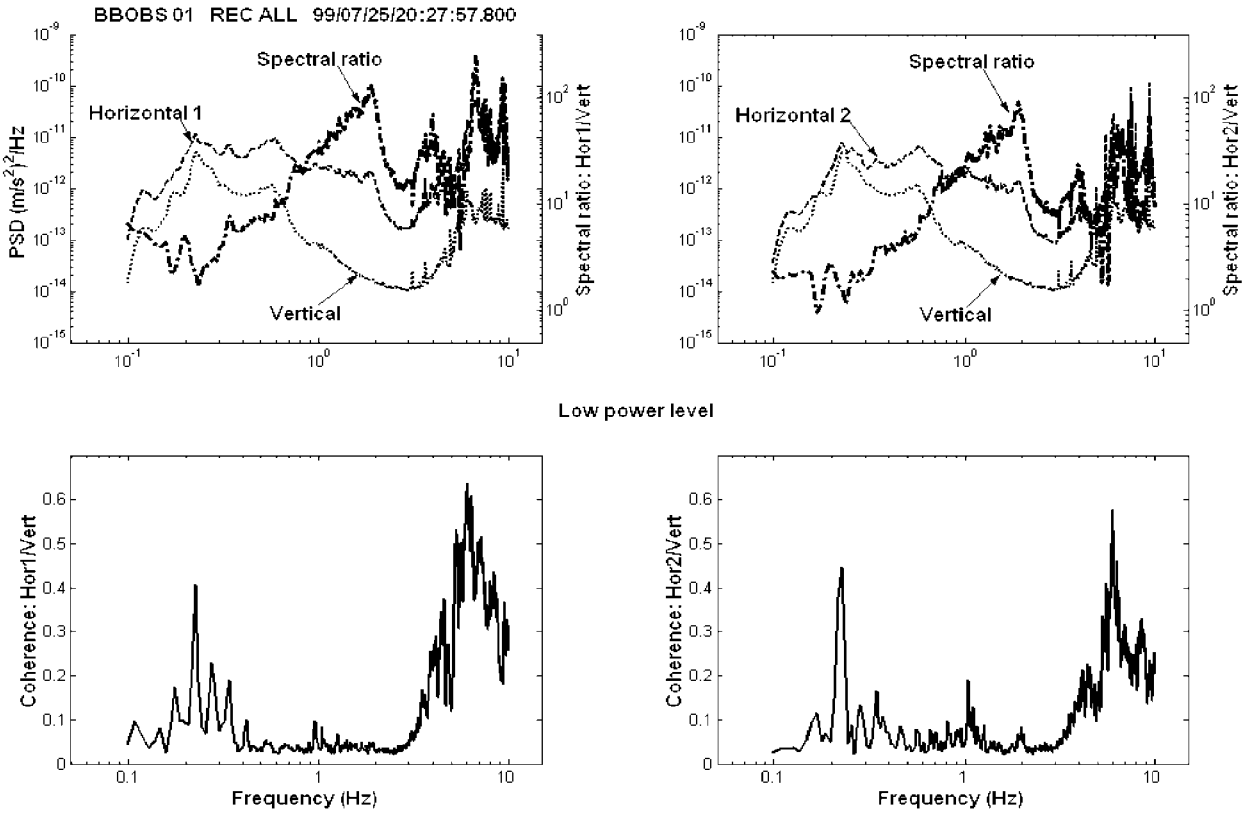

Figure 8. Power spectral density estimates, spectral ratios, and coherence between horizontal and vertical components of background noise measurements for low power level. The high and midpower level cases are very similar and are therefore not shown here.

coupled with *P*-wave signals, affecting high-frequency signals preferentially.

Our preferred model (Table 2) contains shear-wave velocities as low as 90 m/s for the top 5-m-thick layer of the marine sediments and 190 m/sec for the subjacent 10-m-thick layer of sediments. Although the literature is quite sparse on this topic, these values are consistent with soft sediment velocities reported for marine sediments and some nonmarine sites. For example, Rosenblad and Stokoe (2001) used spectral analysis of surface waves to estimate shear-wave velocities of marine sediments in the GOM and off the coast of Vancouver, British Columbia. They report shear-wave velocities of 30.5 m/sec for the topmost 0.5 m and 210 m/sec for the next 9.5-m-thick layer at the GOM site and 44, 98, and 168 m/sec for the top three layers of 1.1, 2.7 and 6.1 m, respectively, at the Vancouver site. Zeldenrust and Stephen (2000) inferred an average shear-wave velocity of 76 m/sec for the shallow sediments at the Ocean Drilling Program (ODP) site 843B (OSN-1), offshore the island of Hawaii. Schultheiss (1985) found, while investigating marine sediments of the DSDP-leg 86 in the Northwest Pacific, shear-wave velocities ranging from a few to 40 m/sec. Schreiner *et al.* (1991) obtained estimates as low as 27–32 m/sec by modeling interface waves at two deepwater sites in the Pacific Ocean. They reported that the velocity gradient in the top 1 m of sediments was 5.2 m/sec/m and 3.1 m/sec/m in the next 100 m at one site. At the second site gradients varied from 5.0 to 8.0 m/sec/m in the top 1 m and from 4.5 to 7.0 m/sec/m in the next 20 m. Richardson *et al.* (1991) used a pulse technique to measure shear-wave velocities at several shallow-water sites near La Spezia, Italy, and found values ranging from 17 m/sec to over 100 m/sec near the sediment-water interface; shear-wave velocity gradients varied from 4 to 17 m/sec m in the upper 2 m of muddy sediments to as high as 85 m/sec/m at a hard-packed sandy site. Finally, the shear-wave velocity model we found for the GOM is consistent with values reported for some nonmarine sites as well. Acosta *et al.* (1993) reported shear-wave velocities between 65 and 90 m/sec in the soft clays of the Mexico City valley.

In contrast to the reports described above, Jensen (1991) modeled shear waves recorded at a site in the Barents Sea, which exhibited unusually high attenuation at the lower end of the recorded frequency spectrum (between 35 and 200 Hz) and found that a model that includes unusually high shear-wave velocities of 500–700 m/sec near the water/seabed interface produces an acceptable fit to the data. Jensen acknowledged that his results are controversial, based on the results of previous studies, and pointed out that the iterative forward-modeling scheme he employed seeks only to find a

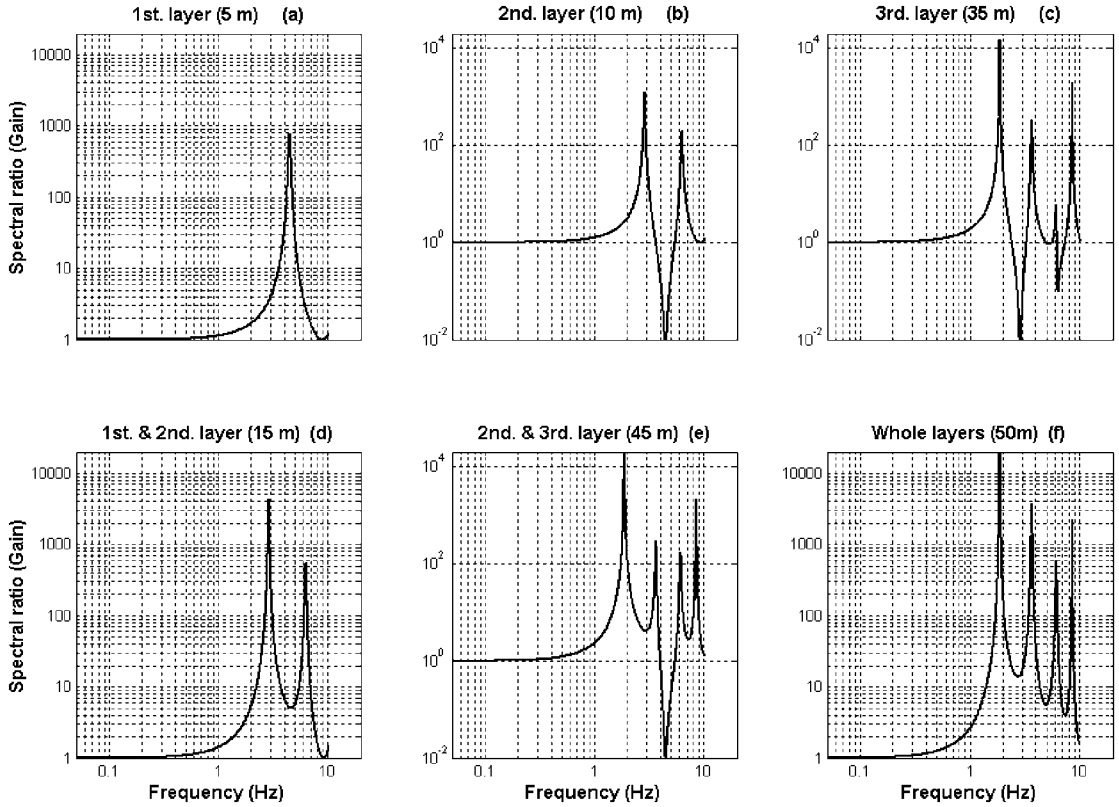

Figure 9. *SH* wave transfer functions of individual layers of 5- (a), 10- (b), and 35-m thickness (c), the cumulative first and second layers (15 m) (d), the second and third layers (45 m) (e), and the whole 50-m, three-layer soil system under a water layer (f).

plausible model; he does not stipulate what particular features, such as shallow fast velocities, are required. It should be noted, as well, that the forward-modeling scheme used here does not identify a unique solution either, nor does it assess uncertainties associated with the best-fitting model. An approach to searching the model space more widely and formally computing uncertainties will be the subject of future work. This new approach, based on global optimization, will allow us to assess uniqueness and whether certain features of a model are required in order to fit the data.

H/V spectral ratios of two of the earthquakes studied, located in the California–Nevada border region and in Nicaragua, respectively, do not show the 3.9 and 6.5 Hz peaks. These peaks are well defined in the H/V spectral ratio obtained with background noise measurements and with data from the earthquakes located in the Gulf of California (magnitude 5.1) and in South America (magnitude 5.9). This discrepancy may be due to directivity effects at the source or a 3D effect in the medium or soil/rock interface at the site. Shear modes in the seafloor sediments due to ambient background noise result from an infrasonic noise field generated in the water column that interacts with the elastic seabed to excite the soft sediments (Godin and Chapman, 1999). The conversion to shear waves occurs most strongly at the largest impedance contrast, generally at the sediment/rock boundary at the base of the sedimentary layer. Multiple transits in the sediment layer by the shear wave give rise to resonances at frequencies that favor constructive interference. Due to its lack of directivity and coherence, the noise field produces relatively independent compressional and shear motions in the sediments. In contrast, waves generated by earthquakes impinge upon the bottom of the soil system from a clear direction, whereupon some *P* energy is converted to *SV*. Any mechanism that serves to enhance the conversion from *P* to *SV* energy will also enhance the overall coherence between time series recorded on horizontal and vertical components, rendering Nakamura's assumption invalid. To enhance this conversion for some earthquakes relative to others requires us to invoke either 3D variations or anisotropy in the medium or directivity of the source mechanism. In this respect, computing ratios from background noise, provided it contains sufficient energy, may be preferable to computing ratios with waves generated by earthquakes.

To evaluate the possibility of a source directivity effect we reviewed focal mechanisms reported in the Harvard's Centroid Moment Tensor and the U.S. Geologic Survey National Earthquake Information Center catalogs. We found that the azimuth to the BBOBS from the Nicaragua event lies very close to a node for *SH* radiation pattern, which would mean that total shear-wave energy arriving at the BBOBS site would be relatively diminished compared with the other earthquakes. However, while the azimuth from the Ecuador

event (which shows peaks at the higher frequency) to the BBOBS does not lie along any nodal lines, neither does the azimuth from the California-Nevada earthquake (which does not show peaks at 3.9 and 6.5 Hz), suggesting that this explanation is incomplete, at best. No moment tensor was available for the relatively small Gulf of California earthquake.

Conclusions

Modeling H/V spectral ratios of data recorded with the newly developed UTIG broadband OBS offers a fast and inexpensive means to obtain information about the preferential vibration modes and physical parameters of soft sediment systems. Transfer functions computed with this information can be used to help design engineering structures such as foundations (30–100 m) for oil drilling and production platforms and pipelines (2–5 m) in deep water. This method makes use of background noise rather than coherent input signals so that it is not necessary to conduct an active-source experiment, nor is it necessary to wait for an earthquake of the appropriate size or in the ideal location. The method is well suited for modeling shallow sediments, which cover the great majority of the seafloor. The broadband OBS is small and lightweight, operates autonomously, and is useful for broadband local, regional, and teleseismic studies as well.

Acknowledgments

This work was supported by Grant Number 003658-225-1997 of the Texas Higher Education Coordinating Board's Advanced Technology Program and DSWA Contract 001-97-I-0016. Carlos I. Huerta-Lopez was supported by a Ewing-Worzel fellowship from the UT Institute for Geophysics during a portion of this project.

References

Abramovich, I. A., M. E. Cobern, A. V. Kharlamov, and A. P. Panferov (2001). Investigation of nonlinearities in vertical sensors of MET seismometers, *Seism. Res. Lett.* **72,** 199–204.

Acosta J., S. Alvarez, L. Mendoza, and G. Arellano (1994). Microzonación del área de Tijuana, B. C. con base en la distribución de períodos dominates del movimiento del suelo. Informe Técnico. Comunicaciones Académicas. Serie Sismología. CICESE, CISIT9402, 34 (in Spanish).

Acosta, J, C. Huerta, L. Mendoza, and A. Reyes (1993). Modelado de la respuesta sísmica en el subsuelo de la ciudad de México, con registros a profundidad. Revista Geofísica Internacional. **32,** 131–152 (in Spanish).

Aki, K. (1988). Local site effects on strong ground motions, in *Earthquake Engineering and Soil Dynamics II—Recent Advances in Ground Motion Evaluation*, J. L. Von Thun (Editor), Geotechnical Special Publication, *Am. Soc. Civil Engr.* **20,** 103–155, New York.

Aki, K. (1993). Local site effects on weak and strong ground motion, *Tectonophysics* **218,** 93–111.

Anderson, J. G., Y. Lee, Y. Zeng, and S. Day (1996). Control of ground motion by the upper 30 meters, *Bull. Seism. Soc. Am.* **86,** 1749–1759.

Bard, P.-Y. (1995). Effects of surface geology on ground motion: recent results and remaining issues, *Proc. of the 10th European Conf. on Earthquake Engineering*, Vienna, Austria, Balkema, Rottherdam **1,** 305–323.

Borcherdt, R. D. (1970). Effects of local geology on ground motion near San Francisco Bay, *Bull. Seism. Soc. Am.* **60,** 29–61.

Field, E. H., and K. H. Jacob (1995). A comparison and test of various site response estimation techniques, including three that are not reference site dependent, *Bull. Seism. Soc. Am.* **85,** 1127–1143.

Frohlich, C. (1982). Seismicity of the central Gulf of Mexico, *Geology* **10,** 103–106.

Godin, O. A., and D. M. F. Chapman (1999). Shear-speed gradients and ocean seismo-acoustic noise response, *J. Acoust. Soc. Am.* **106,** 2367–2382.

Gutenberg, B. (1957). Effects of ground on earthquake motion, *Bull. Seism. Soc. Am.* **47,** 221–250.

Haskell, N. A. (1953). The dispersion of surface waves on multilayered media, *Bull. Seism. Soc. Am.* **73,** 17–34.

Horvath, P., G. V. Latham, Y. Nakamura, and H. J. Dorman (1980). Lunar near-surface shear wave velocities at the Apollo landing sites as inferred from spectral amplitude ratios, *J. Geophys. Res.* **85,** 6572–6578.

Jensen, F. B. (1991). Excess attenuation in low-frequency shallow-water acoustics: a shear wave effect?, in *Proc. of the Conf. on Shear Waves in Marine Sediments*, La Spezia, Italy, 15–19 October 1990, 421–430.

Kanai, K., R. Takahasi, and H. Kawasumi (1956). Seismic characteristics of ground, *Proc. of the World Conf. on Earthquake Engineering*, EERI Berkeley, California, 31-1–31-16.

Kausel, E., and J. M. Roësset (1981). Stiffness matrices for layered soils, *Bull. Seism. Soc. Am.* **71,** 1743–1761.

Lachet, C., and P.-Y. Bard (1994). Numerical and theoretical investigations on the possibilities and limitations of "Nakamura's" technique, *J. Phys. Earth* **42,** 377–394.

Nakamura, Y. (1989). A method for dynamic characteristics estimation of subsurface using microtremor on the ground surface, *Q. R. Railway Tech. Inst.* **30,** 25–33.

Nakamura, Y., and J. Garmany (1991). Development of Upgraded Ocean-Bottom Seismograph. Technical Report 111, March 7, Institute for Geophysics, University of Texas at Austin.

Nakamura, Y., P. L. Donoho, P. H. Roper, and P. M. McPherson (1987). Large-offset seismic surveying using ocean-bottom seismographs and air guns: instrumentation and field technique, *Geophysics* **52,** 1601–1611.

Pulliam, J., Y. Nakamura, C. Huerta-Lopez, and B. Yates (2003). Field test of an inexpensive, small broadband ocean-bottom seismograph, *Bull. Seism. Soc. Am.* **93,** no. 1, 152–171.

Raptakis, D., N. Theodulidis, and K. Pitilakis (1998). Standard spectral ratio and horizontal to vertical ratio techniques: data analysis of the Euroseistest strong motion array in Volvi-Thessaloniki (Greece), *Earthquake Spectra* **14,** 203–224.

Richardson, M. D., E. Muzi, B. Miaschi, and F. Turgutcan (1991). Shear wave velocity gradients in near-surface marine sediments. in *Proc. of the Conf. on Shear Waves in Marine Sediments*, La Spezia, Italy, October 1990, 295–304.

Roësset, J. M., and R. V. Whitman (1969). Theoretical background for amplification studies, Research Report R69-15, Soils Publication No. 231, Department of Civil Engineering MIT, Cambridge, Massachusetts.

Rosenblad, B. L., and K. H. Stokoe II (2001). Offshore shear wave velocity profiling using interface waves, in *Proc. of OTRC International Conf. Honoring Professor Wayne A. Dunlap*, Houston, Texas, April 2001, 15–31.

Satterfield, W., and E. W. Behrens (1990). A late Quaternary canyon/channel system, northwest Gulf of Mexico continental slope, *Mar. Geol.* **92,** 51–67.

Schreiner, A. E., L. M. Dorman, and L. D. Bibee (1991). Shear wave velocity structure from interfase waves at two deep water sites in the Pacific Ocean, in *Proc. of the Conf. on Shear Waves in Marine Sediments*, La Spezia, Italy, 15–19 October 1990, 231–238.

Schultheiss, P. J. (1985). Physical and geotechnical properties of sediments from the Northwest Pacific, Hearth, G. R. and L. H. Burckle, Init. Repts. DSDP, **86,** U.S. Govt. Printing Office, Washington.

Seale, S. H., and R. J. Archuleta (1989). Site amplification and attenuation of strong ground motion, *Bull. Seism. Soc. Am.* **79,** 1673–1696.

Theodulidis, N. P., and P.-Y. Bard (1995). Horizontal to vertical spectral ratio and geological conditions: an analysis of strong motion data from Greece and Taiwan (SMART-I), *Soil Dyn. Earthquake Eng.* **14,** 177–197.

Theodulidis, N. P., P.-Y. Bard, R. Archuleta, and M. Buchon (1996). Horizontal to vertical spectral ratio and geological conditions: the case of Garner Valley Downhole Array in Southern California, *Bull. Seism. Soc. Am.* **86,** 306–319.

Thomson, W. T. (1950). Transmission of elastic waves through a stratified soil medium, *J. Appl. Phys.* **21,** 89–93.

Zeldenrust, I., and R. A. Stephen (2000). Shear wave resonance in sediments on the deep sea floor (abstract), *EOS* **81,** F819.

Institute for Geophysics and Department of Civil Engineering
University of Texas at Austin
4412 Spicewood Springs Road, Bldg. 600
Austin, Texas 78759-8500
huerta@ig.utexas.edu
(C.H.L.)

Institute for Geophysics
University of Texas at Austin
4412 Spicewood Springs Road, Bldg. 600
Austin, Texas 78759-8500
jay@ig.utexas.edu
vosio@ig.utexas.edu
(J.P., Y.N.)

Manuscript received 23 October 2001.